World Academy of Science, Engineering and Technology
International Journal of Mechanical and Mechatronics Engineering
Vol:10, No:2, 2016

One-Dimensional Performance Improvement of a Single-Stage Transonic Compressor

A. Shahsavari, M. Nili-Ahmadabadi

***Abstract*—**This paper presents an innovative one-dimensional optimization of a transonic compressor based on the radial equilibrium theory by means of increasing blade loading. Firstly, the rotor blade of the transonic compressor is redesigned based on the constant span-wise deHaller number and diffusion. The code is applied to extract compressor meridional plane and blade to blade geometry containing rotor and stator in order to design blade three-dimensional view. A structured grid is generated for the numerical domain of fluid. Finer grids are used for regions near walls to capture boundary layer effects and behavior. RANS equations are solved by finite volume method for rotating zones (rotor) and stationary zones (stator). The experimental data, available for the performance map of NASA Rotor67, is used to validate the results of simulations. Then, the capability of the design method is validated by CFD that is capable of predicting the performance map. The numerical results of new geometry show about 19% increase in pressure ratio and 11% improvement in overall efficiency of the transonic stage; however, the design point mass flow rate of the new compressor is 5.7% less than that of the original compressor.

***Keywords*—**One dimensional design, deHaller number, radial equilibrium, transonic compressor.

I. Introduction

IN modern high-performance aircraft engine and gas turbine, transonic compressor stages are major components that even a small improvement in their efficiency and pressure ratio can result in huge saving energy costs; subsequently, recent demands for light and small, in spite of highly loaded compressors has been increasing. Compressor optimization for improving aerodynamic performance was done by several researchers. A preliminary design efficiency optimization of an axial flow compressor using one-dimensional flow theory was introduced by Chen [1]. They presented a new model consists of analytical relations between the isentropic efficiency, flow coefficient, work coefficient, flow angles and degree of reaction. The optimization purpose was to find the flow angles to maximize the isentropic efficiency for fixed values of flow coefficient, velocity coefficients, and some specific constraints. In another paper, Lingen Chen [2] formulated an axial flow compressor design for subcritical Mach numbers as a non-linear multi-objective mathematical program to minimize the aerodynamic losses and the weight of stage and to maximize the compressor stall margin. He also presented a model for the efficiency optimization of multistage axial compressor assuming a fixed configuration for flow path in which one-dimensional flow theory was used [3].

Boiko [4] presented a detailed mathematical model for the optimal design of single and multi-stage axial flow turbines by assuming a fixed distribution of axial velocities or a fixed flow-path shape and obtained the corresponding optimized results. Jin Shik Lim [5] applied the gradient projection method to simulate algorithm which consists of thermodynamic compression relations, cascade geometric variables, empirical loss correlations and simple stress relations for a design program to optimize an axial compressor stage.

By recent advances in CFD, most of the research papers on optimization of turbomachinery blades using this tool have been published. Many of these researchers have used different optimization algorithms to achieve their goal. A multidisciplinary algorithm that incorporates zero and first order optimization techniques were presented by Jmaes A Jones [6]. He used Bezier geometry representation for CFD design to make 3D changes in turbomachinery blade.

Ernesto Benini [7] used a multi-objective evolution algorithm and a three-dimensional Navier-stokes Code (CFX TASCflow®) to maximize the pressure ratio and isentropic efficiency of Rotor_37 in design point by mass flow rate constraint. Akin Keskin [8] show how to automate a given Roles-Royce preliminary design process in order to find Pareto-optimal trade-off solutions for design conditions. A multi-objective numerical optimization was carried out by [9] for axial flow compressor in order to achieve higher adiabatic efficiency and pressure ratio with design variables such as sweep, lean and skew by the three-dimensional RANs flow solver.

A design tool was developed by M. A. Aziz [10] using the correlation of cascade experimental data for the shock losses and deviation angle to select the design parameters for the preliminary design of transonic compressor in order to achieve optimum performance and surge margin. The designed transonic fan was tested and simulated numerically using CFD to verify the developed design tool.

Okui [11] redesigned the camber line, spanwise distribution of sweep and chord length of a moderately transonic compressor rotor by means of a multi-objective optimization, using the differential evolutionary algorithm in combination with an Artificial Neural Network and a 3D Navier stokes solver. In this paper, the two objectives were an increase in efficiency and unchanged stall margin. The best results were

A. Shahsavari (Master of Science student) is with the Isfahan University of Technology, Isfahan, 8415683111 Iran (phone: 0098313915240; fax: 00983133915240; e-mail: ali.shahsavari@me.iut.ac.ir).

M. Nili-Ahmadabadi (Assistant Professor) is with the Department of Mechanical Engineering, Isfahan University of Technology, Isfahan, 8415683111 Iran (e-mail: m.nili@cc.iut.ac.ir).

obtained by increasing blade loading and extra flow turning which is a redistribution of rotor flow.

Rotor blades of NASA Rotor 67 were redesigned through blade profiling by using a viscous adjoint method based on the Reynolds-averaged Navier-Stokes equation and Spalart-Allmaras turbulence model to a multipoint design optimization. Luo [12] suggested a single-point optimization near the peak efficiency point which was able to raise the adiabatic efficiency of blade row at the same pressure ratio and mass flow rate. At the same time, it weakened the shock by replacing a double shock with a single shock. A three-point optimization (stall, peak efficiency, and surge) was applied to gain a broad range of operation.

TABLE I
SYMBOLS USED IN THIS PAPER

Symbol	Quantity	Unit
AR	aspect Ratio	
c	absolute Velocity	m/s
cd	chord	m
DF	diffusion Factor	
dH	de-Haller number	
h	enthalpy	kJ/kg
HTR	hub to tip ratio	
i	incidence angle	degree
m	the mass flow rate	kg/s
P	pressure	Pa
r	radius	m
r_p	the total pressure ratio	
Rn	reaction	
s	entropy	kJ/(kgK)
T	temperature	K
t	the thickness of the blade	m
U	blade velocity	m/s
w	relative velocity	m/s
α	flow angle	degree
β	blade angle	degree
γ	specific heat ratio	
δ	deviation Angle	degree
η	efficiency	
θ	camber angle	degree
ρ	density	Kg/m^3
σ	solidity	
Ψ	loading coefficient	
ω	angular velocity	rad/s
	Subscripts	
0	total properties of the fluid	
1	inlet	
2	outlet	
max	Maximum value	
x	axial direction	
θ	tangential direction	

A global optimization method including Cooperative Co-Evolution Algorithm was used by Song [13] to modify blade stacking line and sectional profiles in order to achieve more overall efficiency and pressure ratio in operating flow range in NASA Rotor 67. The CFD simulation was conducted by ANSYS CFX, and three blade sections were selected to be optimized by choosing 2 Bezier points and 3 control points in every section.

In this paper, an innovative one-dimensional design based on the radial equilibrium and constant de-Haller is presented to redesign compressor for achieving higher pressure ratios and adiabatic efficiency; meanwhile, the parameters such as diameter, angular velocity, inlet tip relative Mach number, blade aspect ratio and blade hub tip ratio are constant. The designed compressor is simulated by a RANS flow solver with SST turbulence model which its results are in good agreement with the obtained results from the preliminary design. The efficiency and the pressure ratio of the newly designed compressor stage are improved significantly. The main focus of this paper is on the rotor design; although, the stator of the new stage is redesigned according to the new flow angles in rotor outlet. All symbols used in this article are introduced in Table I.

TABLE II
SPECIFICATION OF CASE STUDY

Parameter	Value	Unit
Pressure ratio	1.38	
Mass flow rate	3.08	kg/s
Number of Rotor blades	16	
Number of Stator blades	40	
Rotational speed	38300	rpm
Tip relative Mach number	1.15	
Tip clearance	10% of span	m
Isentropic efficiency	79.89%	
Aspect Ratio	1	
Hub Tip Ratio	0.62	
Tip diameter	0.18	m

II. FUNDAMENTAL EQUATIONS

The main idea of this paper is to redesign a single-stage transonic axial compressor based on the constant de-Haller number and radial equilibrium equation to use full diffusion capacity of the whole blade to produce higher pressure ratio and efficiency. (1) and (2) show radial equilibrium equation neglecting radial speed in the outlet flow of compressor rotor. Since it is supposed to design the first stage of an axial compressor; the entropy gradient is neglected [14]. In most of the blade design based on radial equilibrium strategy such as free vortex, the energy addition to the fluid flow inside the rotor is uniform by radius. However, in the present study, this assumption is replaced by a non-uniform energy addition to the fluid flow. Therefore, in (1) and (2), total enthalpy has a radial gradient. Notice that the air is considered as an ideal gas in both theoretical relations and simulation.

$$dh_0/dr = T.(ds/dr) + c_x.(dc_x/dr) + (c_\theta/r).(d(rc_\theta)/dr) \quad (1)$$

$$dh_0/dr = c_x.(dc_x/dr) + (c_\theta/r).(d(rc_\theta)/dr) \quad (2)$$

Considering that entering flow into the first rotor of the compressor has uniform total enthalpy without swirl velocity through the hub to tip inlet, Euler work equations (3) and (2)

are combined to achieve (4) for the rotor outlet.

$$h_{02} - h_{01} = U\,(c_{\theta 2} - c_{\theta 1}) \tag{3}$$

$$\frac{d\,(U.c_{\theta 2})}{dr} = c_{x2}\,\frac{dc_{x2}}{dr} + c_{\theta 2}.\frac{d}{dr}(rc_{\theta 2}) \tag{4}$$

According to the stage velocity diagram of an axial flow compressor which is shown in Fig. 1, the main idea of this design method is that outlet velocity components are obtained based on constant relative velocity ratio or de-Haller number equal to 0.72 [15]-[16]. Therefore, the outlet axial velocity can be obtained from (5).

$$\begin{aligned} c_{x2} &= \sqrt{{w_2}^2 - (U - c_{\theta 2})^2}\ \underrightarrow{w_2 / w_1 = dH > 0.72} \\ c_{x2} &= \sqrt{(dH.w_1)^2 - (U - c_{\theta 2})^2} \end{aligned} \tag{5}$$

By importing (5) into (4), (6) is derived. Then, by simplifying it, (7) and (8) are derived.

$$\begin{aligned} &\frac{d\,(U.c_{\theta 2})}{dr} = \sqrt{(dH.w_1)^2 - (U - c_{\theta 2})^2}\,. \\ &\frac{d}{dr}\left(\sqrt{(dH.w_1)^2 - (U - c_{\theta 2})^2}\right) + c_{\theta 2}.\frac{d}{dr}(rc_{\theta 2}) \end{aligned} \tag{6}$$

$$c_{\theta 2} = r\omega\sqrt{1-(dH)^2} \tag{7}$$

$$c_{x2} = \sqrt{2(r\omega)^2.(dH^2 - 1 + \sqrt{1 - dH^2}) + (dH.c_{a1})^2} \tag{8}$$

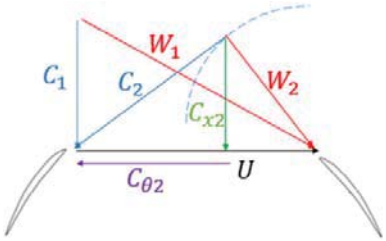

Fig. 1 Stage velocity diagram

Equation (7) shows a force vortex span-wise swirl speed distribution which satisfies the radial equilibrium in spite of constant de-Haller number. Deviation and incidence angles are calculated according to what has been written in [17]. Moreover, optimum solidity is chosen in every section according to stream angles in order to minimize losses [18]. Finally, a computer program based on the algorithm shown in Fig. 2 is developed to calculate all blade geometry and other design parameters. This algorithm first divides span to many sections and then, starts to calculate inlet and outlet flow and blade angles, compressor design and thermodynamic parameters, losses, solidity and finally efficiency. In the end, main outputs are blade thickness-chord wise distribution, blade chord spanwise distribution, blade leading edge and trailing edge profile. Some main results of this program are shown in Figs. 3-6. In these figures, the original geometry is related to the blades of a current axial compressor. The same algorithm is applied for stator design, but here the rotor design algorithm is shown because the main idea of this research is to design rotor with new method and stator is only redesigned to adapt stator blades to new flow angle at rotor outlet.

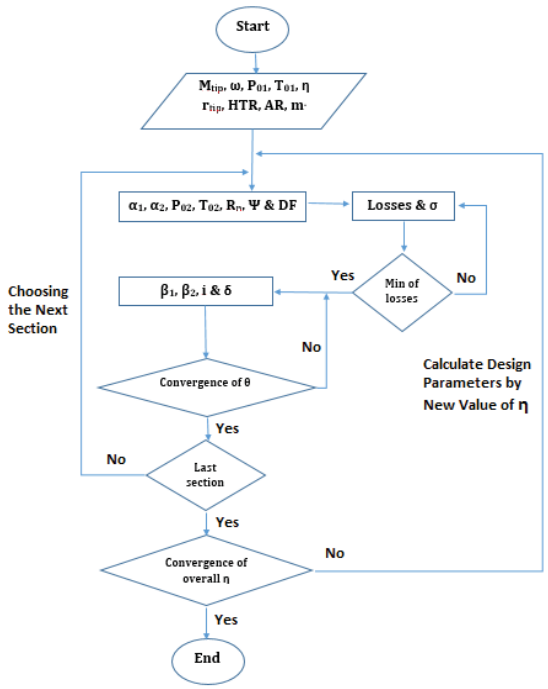

Fig. 2 Design algorithm

Fig. 3 shows blade inlet and outlet angles distribution. New blade design having larger camber angle in comparison to the original geometry represents a higher loading. This outlet angle span-wise distribution is one of the most considerable specifications of new blade geometry. Span-wise constant distribution of diffusion factor (9) and loading factor (11) such as the constant distribution of de-Haller number are other properties of this design method. Simultaneously, reaction defined as (10), is approximately constant and has an acceptable range. Achieving better results in designing axial transonic compressors by redistributing rotor flow and an increase of loading by extra flow turning was mentioned in [11].

Lieblein's diffusion factor relating the peak velocity on the suction surface of blades to the velocity at trailing edge and leading edge [19], is a useful parameter for determining the blade pitch to chord ratio [20].

$$DF = 1 - V_2/V_1 + \Delta V_\theta / 2\sigma V_1 \tag{9}$$

In (9), the relative velocity is used for rotor blades and absolute velocity for stator blades. Diffusion factor over 0.6 are thought to indicate blade stall, and values of about 0.45 are recommended for an efficient design [21]. The diffusion factor of the recent design, according to Fig. 4, is equal to 0.48

which is acceptable.

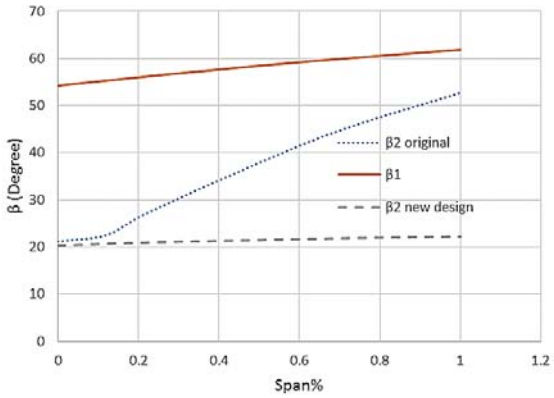

Fig. 3 Blade leading edge and trailing edge angle in new design and original geometry

In compressors, reaction factor which represents the ratio of rotor static enthalpy rise to stage static enthalpy rise is preferred to be around 0.5 [20] which is achieved in new design according to Fig. 4. The reaction is strongly dependent on the flow angles at inlet and outlet of each stage.

$$R_n = (h_2 - h_1)/(h_{02} - h_{01}) \quad (10)$$

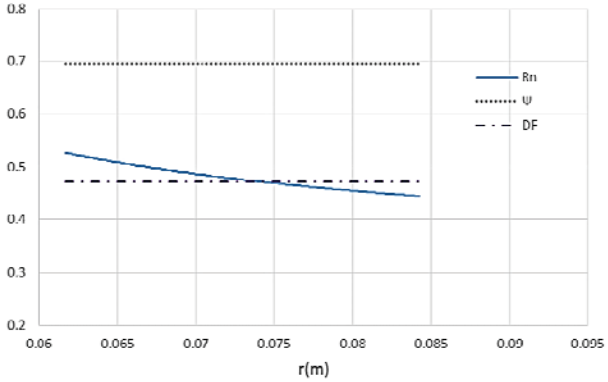

Fig. 4 Design parameters span-wise distribution

Loading represents total enthalpy rise for a special speed of the blade. Designers try to achieve high loaded compressors to reduce the number of stages; however, loading is confined to a maximum because of stall and separation limits.

$$\psi = \Delta h_0 / U^2 \quad (11)$$

For highly loaded axial compressors, it is recommended that maximum loading coefficient is 0.65 [22].

III. Designed Blade Geometry

All sections of the newly designed blade are considered DCA profile and some of its properties are shown in Table III. As shown in Fig. 5, blade sectional profiles for original geometry and newly designed rotor have large differences in both blade inlet and outlet angles, chord length, leading and trailing edge radius and stagger angle. New blades have sharper leading and trailing edge, larger camber angle because of higher loading as expressed later, more chord length and thickness in tip section in comparison with hub sections having narrower blades. Moreover, the stagger angle changes less along a span-wise direction that means new blades has less distortion and can be manufactured more easily.

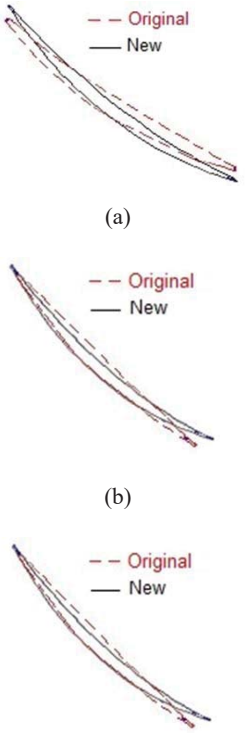

Fig. 5 Comparing new blades and original geometry (a) hub, (b) mid and (c) tip

TABLE III
Specification of Case Study

t_{max}/cd	HTR		AR	r_0/t_{max}
0.05	Inlet=0.62	Outlet=0.74	1	0.06

In Fig. 6, the meridional view of the original geometry and newly designed rotor can be compared. As mentioned, all blade geometry input parameters are the same in both new and original geometry. However, there are many fundamental differences such as less area in new rotor outlet because of higher pressure ratio and higher absolute velocity, distribution of chord which in the new design is larger in tip sections, more blade numbers 25 in the new design in compare to 16 in the original rotor) because of higher loading.

IV. Validation of Simulation

In the present study, CFD simulation is used to prove the performance of new preliminary design technique. The Reynolds-averaged Navier-Stokes equations (RANS) which describe the conservation of mass, momentum, and energy are used in a finite volume method. The Reynolds stress terms in

the momentum transport equations are resolved using shear stress transport (SST) turbulence model, developed to blend the robust and accurate formulation of the k −ω model in the near-wall region with the free-stream independence of the k −ε model in the far field. By using mixing-plane interface model, solution domain is divided into stationary and rotating zones and utilizes relative motion between the various zones to transmit calculated values between zones. To complete the model in rotating zones, Coriolis and centrifugal accelerations are added to momentum equations.

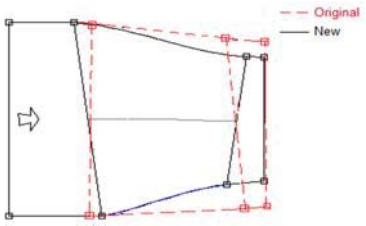

Fig. 6 Meridional view of original compressor geometry and new one

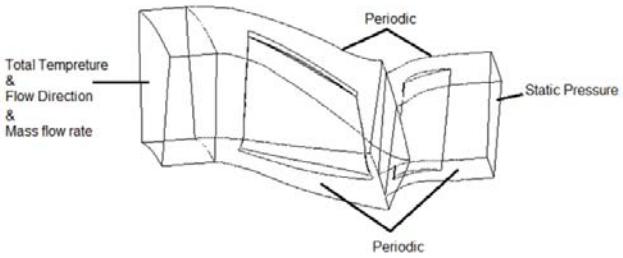

Fig. 7 Boundary conditions used in simulation

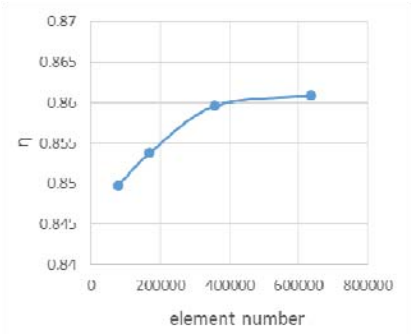

(a)

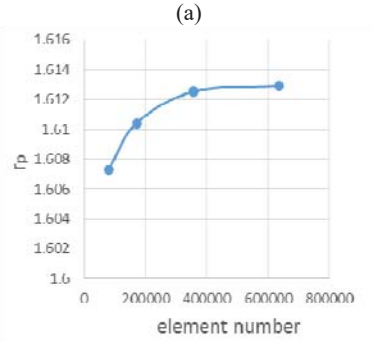

(b)

Fig. 8 Grid study of numerical solution (a) isentropic efficiency and (b) total pressure ratio

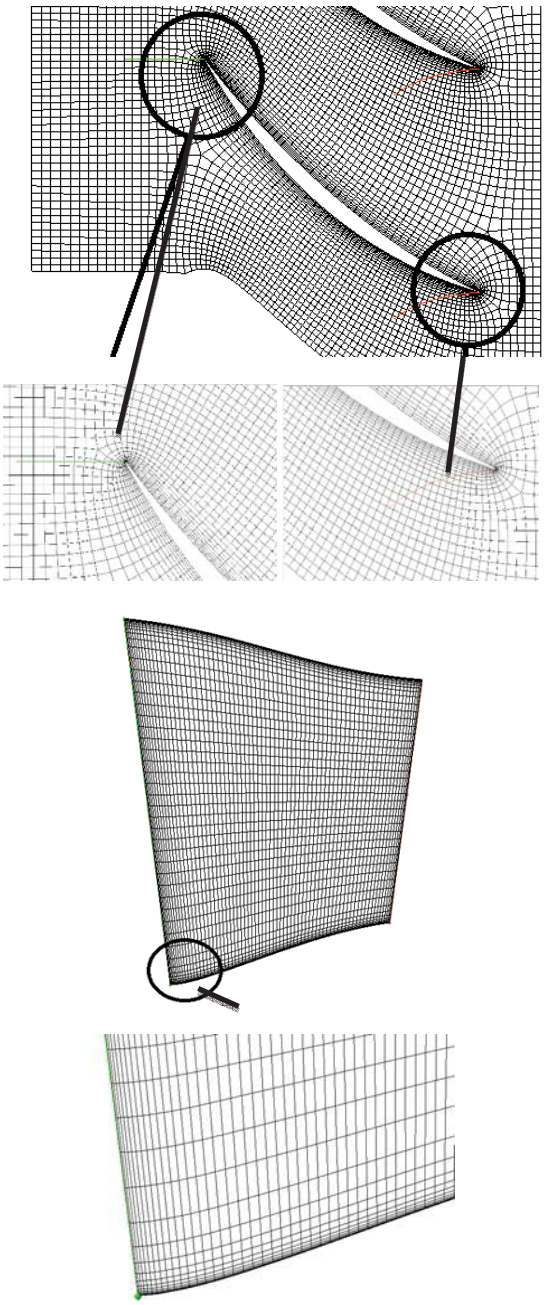

Fig. 9 Computational grid

The mass flow rate, total temperature, and flow direction are specified at the inlet, while static pressure is given at outlet. No-slip and adiabatic conditions are applied to solid surfaces of the blade, hub, and shroud. These boundary conditions are shown in Fig. 7. It is clear that flow is simulated for single blade passage with periodic boundary condition between every two adjacent blades.

The structured grid is used for the numerical domain. To eliminate the influence of grid size, grid dependency is studied. For different resolutions of grids with the same boundary conditions, the evaluated results with two important non-dimensional parameters are shown and compared in Fig. 8.

The compressor pressure ratio and efficiency at nominal flow conditions are taken as the parameters to evaluate four grid configurations and to determine the influence of grid size on the solution. In Fig. 8, it is observed how the calculated compressor pressure ratio and efficiency reach an asymptotic value as the number of elements increases. According to this figure, the grid having 400000 elements is considered to be sufficiently reliable to ensure grid independence. As shown in Fig. 9, the size of element nearby all walls is chosen in a way that the range of y-plus is less than 10.

To verify the results of the numerical method, the performance test data of NASA Rotor67 are compared with the numerical results thereof. Fig. 10 shows the validation results for performance curve of total pressure ratio and adiabatic efficiency defined in (12) and (13).

$$\eta = ((P_{02}/P_{01})^{\frac{\gamma-1}{\gamma}} - 1)\Big/(T_{02}/T_{01} - 1) \tag{12}$$

$$r_p = P_{02}/P_{01} \tag{13}$$

At design point of Rotor 67, the predicted efficiency and pressure ratio are 0.9124 and 1.61, which one is over the measured data of 0.911 and the other is below 1.63, but the discrepancies are small. As observed in Fig. 10, the numerical results are in good agreement with the experimental data.

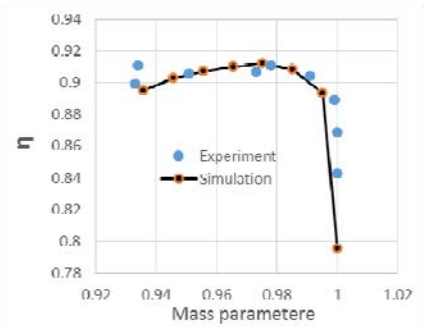

(a)

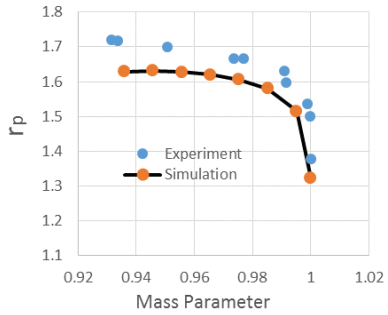

(b)

Fig. 10 Comparisons of predicted and measured overall performance of rotor 67(a) Overall efficiency and (b) Pressure ratio

V. Results and Discussion

Fig. 11 compares the overall performance map of the newly designed blade with that of the original geometry at the design point of each compressor. As shown in this figure, both curves of efficiency and pressure ratio are incredibly above that of the original compressor, which indicates constant diffusion design method improves not only design point performance but also off design performance. Overall efficiency and pressure ratio of the newly designed geometry at design point is respectively 11% and 19% higher than that of the original geometry. However, as an undesirable result, the performance range of the newly designed compressor has been limited. The design point mass flow rate of the newly designed compressor is just about 5.7% less than that of the original one. Reduction in design point mass flow rate is probably caused by two main reasons. First, more blade number of the newly designed geometry leads to a smaller throat and causes more blockage. Second, more axial velocity in rotor outlet causes the flow to be chocked in less mass flow rate and consequently design point mass flow rate decreases [23].

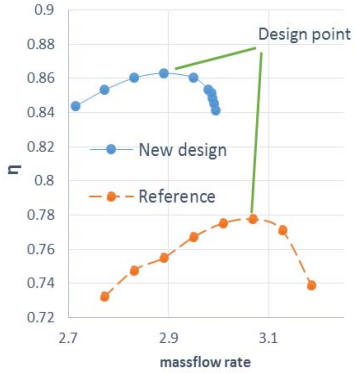

(a)

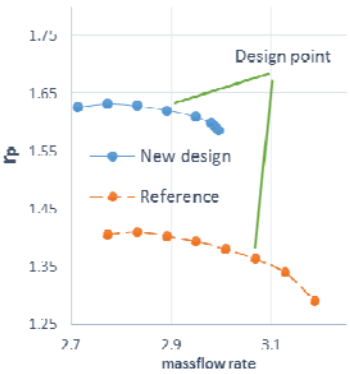

(b)

Fig. 11 Compressor map of reference and new design used in simulation (a)Overall efficiency and (b) Pressure ratio

Fig. 12 indicates absolute velocity component in rotor outlet of the newly designed compressor obtained from theoretical relations and numerical simulation and then, compares them to which obtained from numerical simulation of the original compressor. By comparing theoretical absolute velocity to the simulation result of the new compressor, it is completely obvious that there is the main difference between them

because of no considering blade tip clearance in theoretical analysis. Moreover, in Fig. 12, the rotor outlet absolute velocities of the new and original compressor obtained from the numerical simulation are compared with each other.

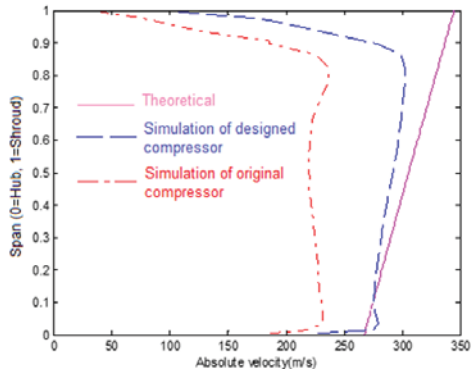

Fig. 12 Comparing theoretical and simulation absolute velocity in Rotor outlet

As shown in Fig. 12, the new compressor has a higher absolute velocity everywhere, especially near the tip section. It means that at the rotor outlet, there is a higher kinetic energy and consequently higher total pressure and overall efficiency as shown in Figs. 13 and 14. Therefore, by using new design method, an evident increase in efficiency and pressure ratio is produced over the entire span.

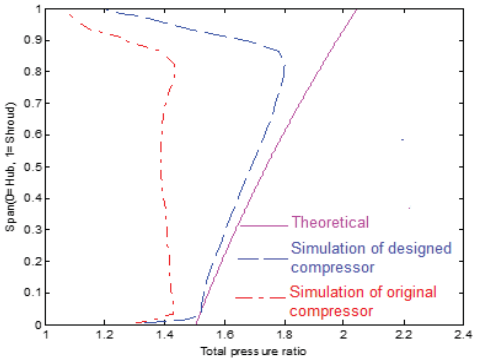

Fig. 13 Comparing theoretical and simulation total pressure in Rotor outlet

As mentioned before, the constant axial velocity at rotor inlet was one of the main assumptions for calculating the radial equilibrium equation. After numerical simulation of the new and original compressor, the inlet velocity distribution is calculated for both cases as shown in Fig. 15. The figure represents a good accuracy of this assumption; however, there is a negligible non-uniformity from mid to tip section.

Figs. 16-18 present the distribution of relative Mach number in different blade's spans at the design point. Differences between relative Mach number in these figures are significant. One of the main differences is shock structure. The shock waves of the new geometry are weaker and more oblique than that of the original one. Decreasing Mach number is another difference in the blade passage of the new geometry which illustrates loss reduction.

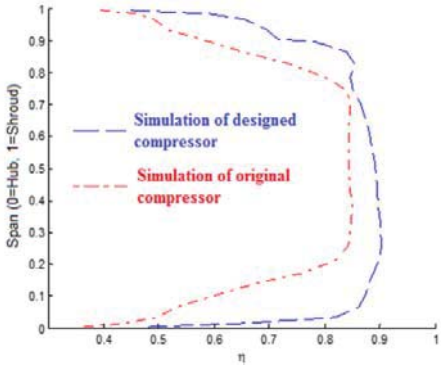

Fig. 14 Comparing isentropic efficiency distribution in stage outlet

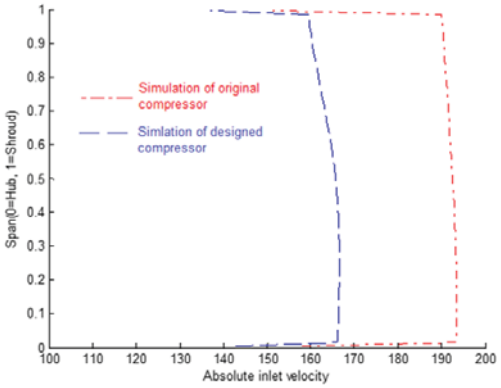

Fig. 15 Absolute velocity in rotor inlet

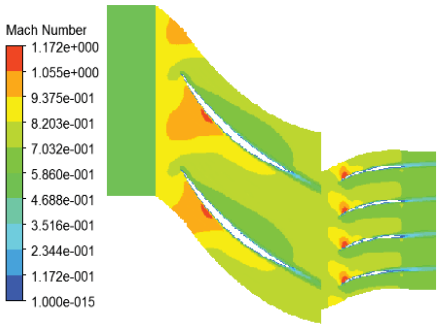

(a)

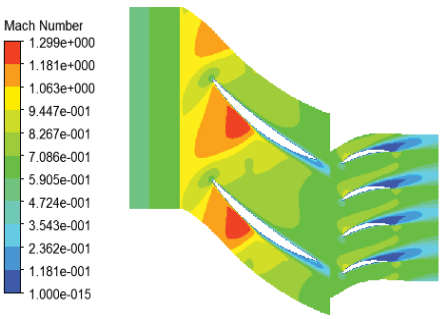

(b)

Fig. 16 Relative Mach number contours 10% span a) New design (b) Original geometry

Fig. 19 represents total pressure contour on the blade to blade section of mid-span. The total pressure difference between the inlet and outlet of the designed compressor is higher than that of the original one. Moreover, the regions with flow losses have been removed in the newly designed compressor relative to the original one.

As shown in Fig. 20, total pressure span-wise distribution for the new and original compressor is compared. As obvious, flow losses near the blades hub and tip are weakened in the new compressor relative to the original one. In other words, the new compressor has a higher total pressure at the stage outlet that causes the stage total pressure ratio to increase. This higher total pressure ratio is due to increase in kinetic energy of air flow at the outlet especially at the top half of the blades.

In Figs. 21-23, the pressure distribution of three blade sections at design point are shown for the new and original rotor. In all sections, static pressure increases. Moreover, the integral of the pressure difference between suction and pressure side for the new rotor is greater than that for the original one because of higher blade loading.

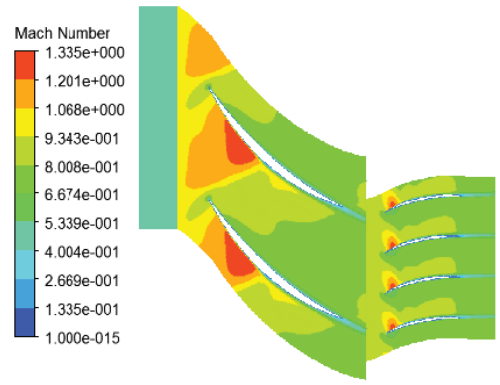

(a)

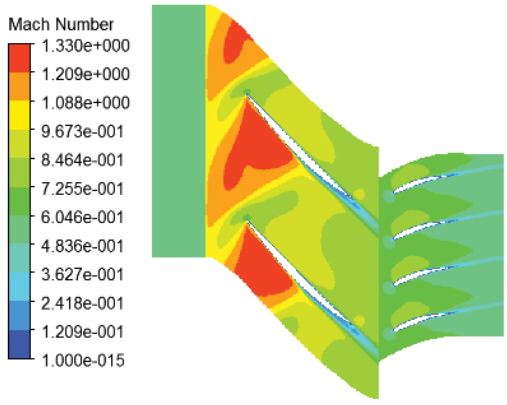

(b)

Fig. 17 Relative Mach number contours 50% span(a) New design and (b) Original geometry

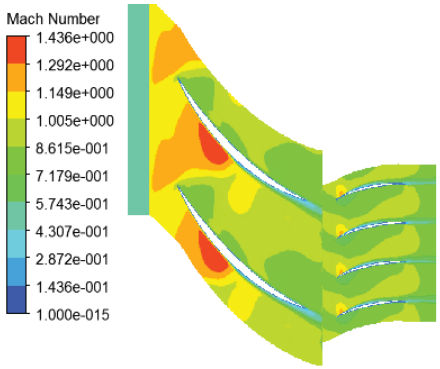

(a)

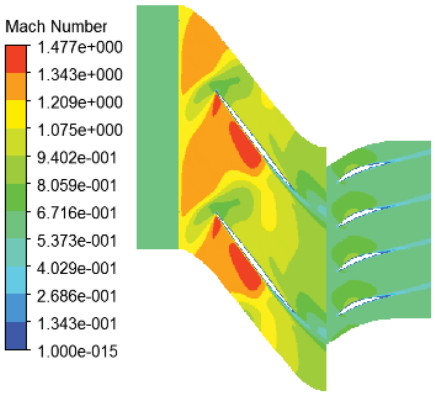

(b)

Fig. 18 Relative Mach number contours 85% span (a) New design and (b) Original geometry

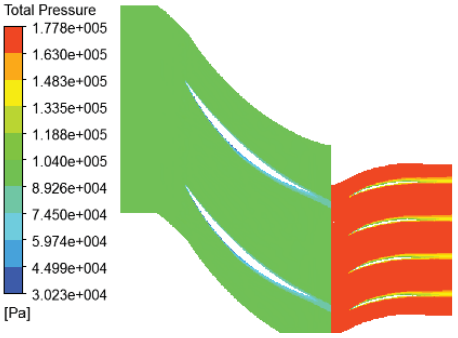

(a)

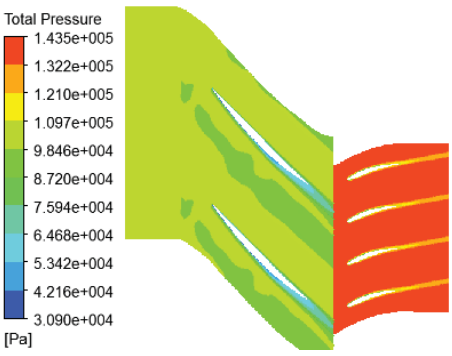

(b)

Fig. 19 Total pressure contours 50% span (a) New design and (b) Original geometry

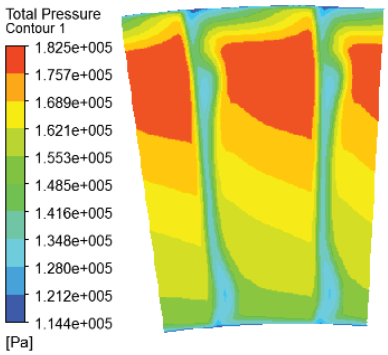

(a)

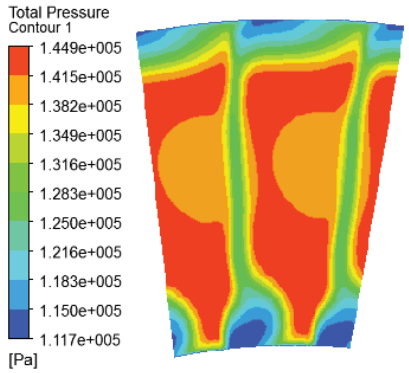

(b)

Fig. 20 Total pressure contours in stage outlet (a) New design and (b) Original geometry

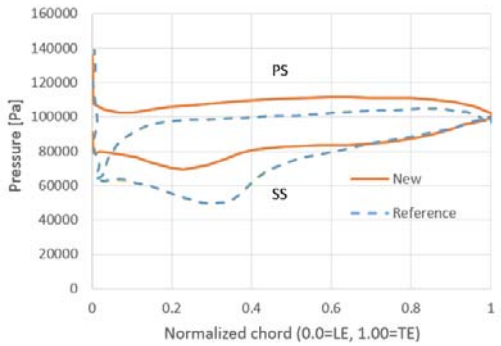

Fig. 21 Static pressure distribution around blade at 10% span

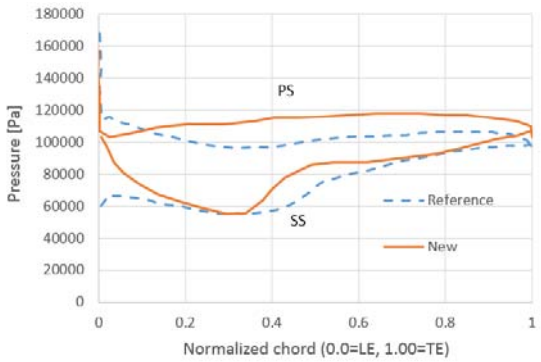

Fig. 22 Static pressure distribution around blade at 50% span

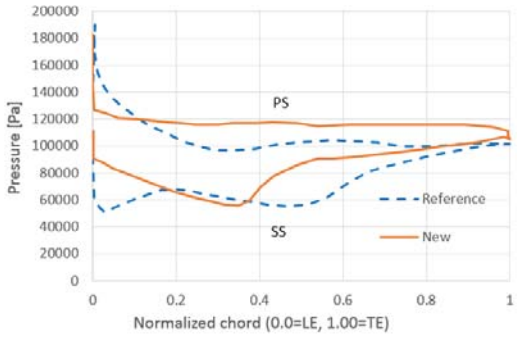

Fig. 23 Static pressure distribution around blade at 85% span

VI. Conclusion

A new design method was developed to improve the performance of transonic compressor geometry. For this, a design code was implemented for the preliminary design based on a constant diffusion to increase blade loading and pressure ratio of the compressor. This code extracted thermodynamic parameters, compressor framework, velocity diagrams, blade angles and a scheme of a meridional section of a new compressor. The new geometry was simulated by the viscous turbulent solver. The CFD results such as velocity distribution both in rotor inlet and outlet correlated well with the preliminary design. The results of numerical simulation demonstrated significant improvement, about 11% in overall efficiency and 19% in total pressure ratio. Shifting the surge line in comparison with original geometry showed that the performance at low mass flow rate was improved. In spite of all the mentioned advantages of the newly designed compressor, the less design mass flow rate which was probably caused by the rotor blockage and more axial velocity at the rotor outlet was not desirable.

References

[1] Chen, L., Luo, Jun., Sun, Fengrui., Wu, Chih., *Optimized efficiency axial-flow compressor.* Applied energy, 2005. 81(4): p. 409-419.

[2] Chen, L., F. Sun, and C. Wu, *Optimum design of a subsonic axial-flow compressor stage.* Applied energy, 2005. 80(2): p. 187-195.

[3] Chen, L., Luo, Jun., Sun, Fengrui., Wu, Chih., *Design efficiency optimization of the one-dimensional multi-stage axial flow compressor.* Applied Energy, 2008. 85(7): p. 625-633.

[4] Boiko, A., *Optimal Design for Flow-Path of Axial Turbines.* 1982, Harkov: Higher Education Press.

[5] Lim, J.S. and M.K. Chjng, *Design point optimization of an axial-flow compressor stage.* International journal of heat and fluid flow, 1989. 10(1): p. 48-58.

[6] Jones, J.A., *A multidisciplinary algorithm for the 3-D design optimization of transonic axial compressor blades.* 2002.

[7] Benini, E., *Three-dimensional multi-objective design optimization of a transonic compressor rotor.* Journal of propulsion and power, 2004. 20(3): p. 559-565.

[8] Keskin, A. and D. Bestle, *Application of multi-objective optimization to axial compressor preliminary design.* Aerospace science and technology, 2006. 10(7): p. 581-589.

[9] Samad, A., and K.-Y. Kim, *Multi-objective optimization of an axial compressor blade.* Journal of Mechanical Science and Technology, 2008. 22(5): p. 999-1007.

[10] Aziz, M., F.M. Owis, and M. Abdelrahman, *Preliminary design of a transonic fan for a low by-pass turbofan engine.* International Review of Aerospace Engineering (IREASE), 2013. 6(2): p. 114-127.

[11] Okui, H., Verstraete, Tom., Van Den Braembussche, RA., Alsalihi, Zuheyr., *Three-dimensional design and optimization of a transonic rotor*

in axial flow compressors. Journal of Turbomachinery, 2013. 135(3): p. 031009.
[12] Luo, J., C. Zhou, and F. Liu, *Multipoint design optimization of a transonic compressor blade by using an adjoint method.* Journal of Turbomachinery, 2014. 136(5): p. 051005.
[13] Song, P., J. Sun, and K. Wang. *Blade Shape Optimization of Transonic Axial Flow Fan in Terms of Sectional Profiles and Stacking Line*.in *ASME Turbo Expo 2014: Turbine Technical Conference and Exposition*. 2014. American Society of Mechanical Engineers.
[14] Hatch, J.E., C.C. Giamatti, and R.J. Jackson, *Application of radial-equilibrium condition to axial flow turbomachine design including consideration of a change of entropy with radius downstream of blade row*. 1954, DTIC Document.
[15] Klapproth, J.F., *A review of supersonic compressor development.* Journal of Engineering for Gas Turbines and Power, 1961. 83(3): p. 258-268.
[16] Wennerstrom, A.J., *Design of highly loaded axial-flow fans and compressors*. 2000.
[17] Johnsen, I.A., and R.O. Bullock, *Aerodynamic Design of Axial-Flow Compressors. NASA SP-36.* NASA Special Publication, 1965. 36.
[18] Kerrebrock, J.L., *Flow in transonic compressors.* AIAA Journal, 1981. 19(1): p. 4-19.
[19] Falck, N., *Axial Flow Compressor Mean Line Design.* Master's thesis, Lund University, Lund, Sweden, 2008.
[20] Dixon, S.L. and C. Hall, *Fluid mechanics and thermodynamics of turbomachinery*. 2013: Butterworth-Heinemann, pp. 95–132.
[21] Aungier, R. H. (2003). Axial-Flow Compressors. *American Society of Mechanical Engineers, New York.*
[22] Dickens, T. and I. Day, *The design of highly loaded axial compressors.* Journal of Turbomachinery, 2011. 133(3): p. 031007.
[23] Seyler, D. and L. Smith Jr, *Single stage experimental evaluation of high Mach number compressor rotor blading, Part I, Design of rotor blading.* NASA CR-54581, 1967: p. 26-28.